Accurate estimation of spin-orbit torque in heavy-metal multilayers with account of thermoelectric effects

Enze Zhang,[1,2,*] Shouguo Zhu,[1,2,*] Weihao Li,[1,2] Xin Lin,[1,2] Yongcheng Deng,[1,2]
Xionghua Liu,[1,2,†] and Kaiyou Wang[1,2,3,‡]
[1]*State Key Laboratory for Superlattices and Microstructures, Institute of Semiconductors, Chinese Academy of Sciences, Beijing 100083, China*
[2]*Center of Materials Science and Optoelectronics Engineering, University of Chinese Academy of Sciences, Beijing 100049, China*
[3]*Center for Excellence in Topological Quantum Computation, University of Chinese Academy of Science, Beijing 100049, China*

(Received 15 March 2023; revised 11 May 2023; accepted 15 June 2023; published 27 June 2023)

Heavy metal (HM) multilayers with opposite spin-Hall angle have attracted extensive attentions due to their rich physical properties and controversial reported results. Here, we systematically investigated the spin-orbit torque (SOT) efficiency in $Ta(1)/[Pt(t_{Pt})/Ta(1-t_{Pt})]_5/Pt(1.3)/Co$ multilayers using harmonic Hall voltage response methods. We observed that the SOT efficiency of Pt/Ta multilayer can be continuously tuned with varying Pt or Ta thickness, and the strong thermoelectric effect in Pt/Ta multilayers causes a large mismatch of low-field and high-field harmonic results. Combined with finite element analysis, we demonstrated the enhanced thermoelectric effect in Pt/Ta multilayers originates from the increased resistivity of HM layers and shunt effect, as well as the change of anomalous Nernst coefficient. Furthermore, the accurate SOTs strength can be obtained by ruling out the thermoelectric effect. Our work not only confirms the importance of thermoelectric effect in electrical transport measurements, but also holds significant implications for the precise determination of SOT strength and the application of SOT devices.

DOI: 10.1103/PhysRevB.107.214440

Current-induced spin-orbit torques (SOTs) have attracted considerable attentions due to its great potential in fast operation, low-power consumption, and high-density storage [1–5]. In heavy metal/ferromagnetic (HM/FM) heterostructures, spin currents generated by either spin-Hall effect (SHE) [2,6,7], Rashba effect [1,8], topological surface state [9] or other spin-orbit related mechanisms [10] can effectively manipulate the magnetization of FM layer through SOTs. For the development of SOT devices, it is of great significance to quantitatively measure and improve the strengths of SOTs, especially the dampinglike torque which plays a key role in magnetization switching. As dampinglike torque efficiency can be expressed as $\xi_{DL} \propto T_{\rm int}\sigma_{SH}\rho_{xx}$, where ρ_{xx}, σ_{SH}, and $T_{\rm int}$ are the HM's resistivity, spin-Hall conductivity and interface spin transparency, respectively, thus recent efforts have attempted to enhance ξ_{DL} via doping, inserting submonolayers or interfacial engineering [11–13], in which how to accurately determine SOT strength is an important research issue.

Furthermore, the typical HMs Pt and Ta, with opposite spin polarizations, have been widely investigated in spintronics [2,14–16]. Notably, the research combining Pt and Ta or other two HMs with opposite spin polarizations is rare and mainly focuses on bilayer rather than multilayer systems [17–19]. Meanwhile, the controversial results of Pt/Ta bilayer system are also reported. Ma *et al.* found field-free switching when compensating the torques of Pt and Ta [18], while He *et al.* observed continuously tunable SOT strength and direction with varying Pt/Ta thicknesses but no field-free switching for compensated torques of Pt and Ta [17].

To make clear the influence of combining Pt and Ta on the SOT strength, we designed $Ta(1)/[Pt(t_{Pt})/Ta(1-t_{Pt})]_5/Pt(1.3)/Co$ multilayers and investigated their dampinglike efficiency using harmonic Hall voltage response (HHVR) techniques. We demonstrated the contradictory results for SOT measurements can be eliminated through excluding thermoelectric effect. Our work provides a spin-Hall material system that can continuously tune SOT and Dzyaloshinskii-Moriya interaction (DMI) strength and verifies the remarkable thermoelectric effect in HM/FM systems, which would be very important to deeply understand the nature of SOT.

The stack structures of multilayer samples $Ta(1)/[Pt(t_{Pt})/Ta(1-t_{Pt})]_5/Pt(1.3)/Co(0.8)/Ru(3)$ (thickness in nanometers) with $t_{Pt} = 0$, 0.5, 0.6, 0.7, 0.8, 0.9, Pt (5)/Co (0.8)/Ru (3), and W (5)/CoFeB (1)/ MgO (1.2)/Ta (3) were deposited on Si/SiO_2 substrates by magnetron sputtering at room temperature. The base pressure was less than 1×10^{-8} Torr before deposition [20]. The bottom Ta layer (1 nm) was an adhesion layer and the top Ru or Ta layers were used for capping layer. The W (5)/CoFeB (1)/MgO (1.2)/Ta (3) film was annealed at 350 °C for 1 h in vacuum (F800-35, East Changing Technologies, China) to obtain the perpendicular magnetic anisotropy (PMA). The films were patterned into Hall bar devices by the photolithography and Ar-ion etching for transport measurements. The Kerr characterization of magnetization was taken using a NanoMoke3 magneto-optical Kerr magnetometer and the saturation magnetization (M_S) value of samples were measured

*These authors contributed equally to this work.
†Corresponding author: xionghualiu@semi.ac.cn
‡Corresponding author: kywang@semi.ac.cn

 ©2023 American Physical Society

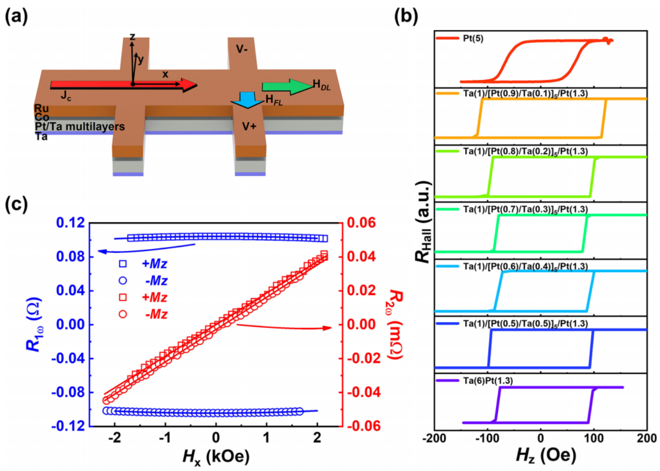

FIG. 1. (a) Geometry and coordinate for Hall measurements of $Ta(1)/[Pt(t_{Pt})/Ta(1-t_{Pt})]_5/Pt(1.3)/Co(0.8)/Ru(3)$ samples. (b) Anomalous Hall resistance R_{Hall} versus the out-of-plane magnetic field H_Z for different t_{Pt} samples. (c) First harmonic resistance $R_{1\omega}$ and second harmonic resistance $R_{2\omega}$ as a function of in-plane field H_x for the sample with $t_{Pt} = 0.9$.

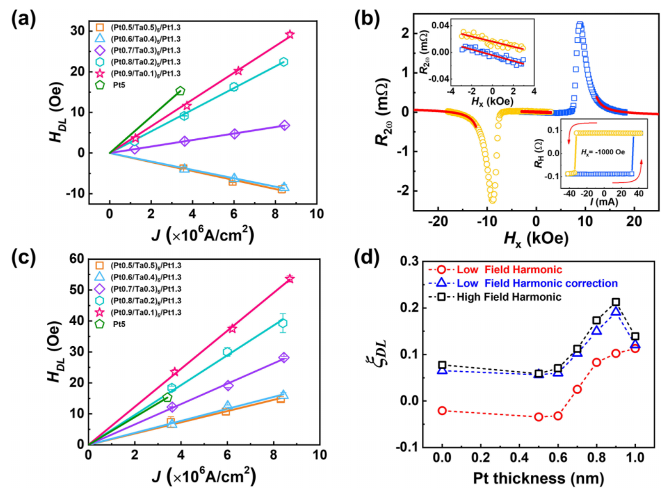

FIG. 2. (a) The dampinglike field as a function of current density for different t_{Pt} samples by low-field harmonic method. (b) Second harmonic resistance $R_{2\omega}$ versus in-plane field for $Ta(1)/[Pt(0.5)/Ta(0.5)]_5/Pt(1.3)/Co(0.8)/Ru(3)$ sample. The upper left corner is the extracted low-field harmonic signal, and the lower right corner is the SOT switching curve. (c) The dampinglike field as a function of current density for different t_{Pt} samples by low-field harmonic correction. (d) ξ_{DL} dependence of Pt thickness.

by vibrating sample magnetometry (Quantum Design). The Hall measurements were performed at room temperature using a Keithley 6221 current source and a Stanford SR830 lock in amplifier. The SOT switching measurements were carried out with Keithley 6221 as the source meter and Keithley 2182A as the nanovoltmeter. The pulse current width is 50 μs and the test current is 0.1 mA to minimize the thermal effect.

Figure 1(a) shows the transport measurement method and coordinates for $Ta(1)/[Pt(t_{Pt})/Ta(1-t_{Pt})]_5/Pt(1.3)/Co(0.8)/Ru(3)$ samples with different thick Pt layer. It is observed that the anomalous Hall resistance (R_{AHE}) as a function of out-of-plane magnetic field (H_z) curves for all the samples exhibit good PMA characteristics [Fig. 1(b)]. We then investigated the SOTs of all Pt/Ta multilayer samples by low-field harmonic method (see Sec. S1 in the Supplemental Material) [21,22]. Figure 1(c) presents the first and second harmonic resistances ($R_{1\omega}$ and $R_{2\omega}$) versus in-plane field (H_x) for the sample with $t_{Pt} = 0.9$. Then the current-induced dampinglike and fieldlike SOT fields can be determined by $H_{DL(FL)} = -2(\partial R_{2\omega}/\partial H_{x(y)})/(\partial^2 R_{1\omega}/\partial^2 H_{x(y)})$ and the corresponding dampinglike (fieldlike) torque efficiency can be obtained via $\xi_{DL(FL)} = 2e\mu_o M_S t_{FM} H_{DL(FL)}/\hbar J$, where t_{FM} and M_S are the thickness and saturated magnetization of FM layer ($\approx 1280\,\mathrm{emu/cm^3}$ for all Pt/Ta multilayer samples).

The calculated H_{DL} with current density (J) for different Pt thick samples is shown in Fig. 2(a). One notes that the slope gradually decreases with decreasing Pt thickness and changes the sign for $t_{Pt} = 0.6$, which means the net spin currents may vary from Pt-dominated to Ta-dominated with increasing Ta thickness [17,19] because of the opposite spin-Hall angles for Pt and Ta. However, as shown in Fig. 2(b), the high-field harmonic signal for samples with $t_{Pt} \leqslant 0.6$ still have positive peaks in positive field, implying the net spin current is still Pt-dominated (see harmonic results of W/CoFeB/MgO and Pt/Co/Ru in Sec. S2 in the Supplemental Material) [22,23], even for the sample with $t_{Pt} = 0$, i.e., Ta (6)/Pt (1.3) bilayer. Moreover, the SOT switching measurement exhibiting anticlockwise under $H_x = -1000$ Oe also confirms the Pt-dominated net spin current, see the inset (right corner) of Fig. 2(b).

To clarify this problem, we took into account the thermoelectric effect. For low-field harmonic method, besides the current-induced effective fields, the thermal gradient of x and z direction ∇_T^x and ∇_T^z can also contribute second signals $R_{\nabla_T}^x$ and $R_{\nabla_T}^z$, which may lead to contradictory results, but this was always ignored before. We employed the high-field HHVR to distinguish the dampinglike field and thermoelectric effect through their different field dependence. For high-field harmonic measurement, when H_x is larger than the effective magnetic anisotropy field H_k, second harmonic resistance can be expressed by $R_{2\omega} = \frac{R_{AHE}}{2}\frac{H_{DL}}{|H_x|-H_k} + R_{\nabla_T}^z \frac{H_x}{|H_x|} + R_{offset}$ (1), where the R_{offset} is the offset signal. Therefore $R_{\nabla_T}^z$ can be quantitatively extracted by fitting Eq. (1). H_k was estimated from the first harmonic signal using the formula $R_{1\omega} \approx R_{AHE}(1 - H_x^2/2H_k^2)$ (see Sec. S3 in the Supplemental Material) [22]. The planar Hall resistance (R_{PHE}) term was not considered because it is small for Pt/Ta multilayers and does not affect our conclusion (see Sec. S4 in the Supplemental Material) [22,24]. Moreover, during the harmonic measurements, the external field was slightly tilted off film plane (~0.5°) to prevent the formation of magnetic domains. We repeated the harmonic measurements while slightly changing the magnitude and direction of the tilt angle. The slight misalignment of external magnetic field has small impact on the fitting results, which confirms the effectiveness of this method (see Sec. S5 in the Supplemental Material) [22].

Figure 2(c) shows H_{DL} *vs* J curves after deducting thermoelectric effects, which is in good agreement with the results of high-field harmonic results (see Sec. S6 in the Supplemental Material) [22], further confirming the contradictory results in

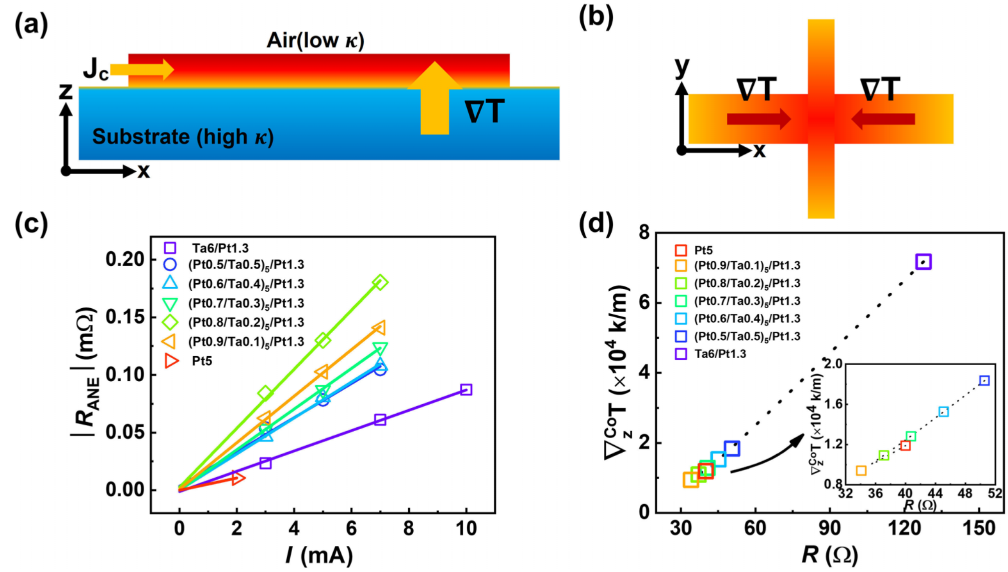

FIG. 3. Schematic diagram of current-induced out-of-plane thermal gradient (a) and in-plane thermal gradient (b) in electrical transport measurements. (c) Linear dependence of $|R_{\mathrm{ANE}}|$ on the current for different Pt thickness samples. (d) The dependence of Co layer temperature gradient on the resistance of HM layers with different t_{Pt} obtained from the results of finite element analysis.

Figs. 2(a) and 2(b) are indeed caused by the thermoelectric effects. Therefore, the good linear dependence of H_{DL} on J in previously work suggested a minor Joule heating effect could be inappropriate because the thermoelectric effect on H_{DL} is also linearly dependent on J (see Sec. S1 of the Supplemental Material) [21,22]. We summarized the ξ_{DL} of samples with different t_{Pt} in Fig. 2(d). It is found that the ξ_{DL} enhances quickly from 0.14 (pure Pt) to maximum 0.19 for $t_{\mathrm{Pt}} = 0.9$ and gradually reduces until approximately saturating to 0.06 for $t_{\mathrm{Pt}} = 0.6$.

We then discussed the influence of Pt thickness on the dampinglike efficiency. To simplify the analysis, we assume the resistivity of HM layer remains constant and the interface is ideal. According to the SHE theory, considering drift-diffusion approximation, the ξ_{DL} and thickness of HM layer satisfies $\xi_{DL}(t_{HM}) = \xi_{DL,\max}[1 - \mathrm{sech}(t_{HM}/\lambda_s)]$, where λ_s and t_{HM} are spin-diffusion length and effective thickness of HM layer, respectively [25]. With increasing t_{HM}, ξ_{DL} is expected to initially increase quickly ($t_{HM} < \lambda_s$) and then saturate slowly [$(t_{HM} \geqslant 3\lambda_s)$], reflecting the nature of bulk effect of SHE. In Pt/Ta multilayer samples, the dominant spin source is Pt ($\lambda_s \approx 2$ nm) with low resistivity (≈ 18 μΩ cm) rather than Ta with high resistivity (≈ 450 μΩ cm). Therefore, the higher Pt content is expected to yield greater ξ_{DL}. Moreover, the resistivities of multilayers increase significantly with decreasing Pt thickness, see Sec. S7 in the Supplemental Material [22]. Therefore, the maximum ξ_{DL} of 0.19 for $t_{\mathrm{Pt}} = 0.9$ can be attributed to a combination of higher Pt content and increased resistivity. With further reducing t_{Pt}, two effects occur simultaneously: firstly, the gradual decrease of Pt results in a decrease in σ_{SH} of Pt; secondly, since Ta has an opposite sign of σ_{SH}, the increase of t_{Ta} will compensate the net spin, which gradually reduces ξ_{DL} to 0.06 for $t_{\mathrm{Pt}} \leqslant 0.6$ [16,26]. Significantly, ξ_{DL} is not fully compensated by Ta even for the sample with $t_{\mathrm{Pt}} = 0$ because of strong shunt effect caused by high resistivity Ta and low resistivity Pt. The approximate saturation of ξ_{DL} at $t_{\mathrm{Pt}} \leqslant 0.6$ can be viewed as a delicate tradeoff between Pt content reduction (reduced dampinglike effective field) and enhanced resistivity (reduced current density in the HM layer) considering parallel resistance model.

In contrast to the in-plane HHVR, the out-of-plane low-field HHVR cannot easily separate the thermoelectric signal for the system with strong thermal effect [27]. Recently, Zhu *et al.* and Shirokura *et al.* reported that the low-field harmonic is significantly underestimated or overestimated due to thermoelectric effects in $(\mathrm{HM/FM})_n$ multilayer structures [28,29]. To accurately determine the SOT's strength, we next discussed the mechanism of thermoelectric effect in Pt/Ta multilayers. When considering ∇_T^z, the electric field $E_{\mathrm{ISHE}} = D_{\mathrm{ISHE}} J_s \times \sigma$ due to longitudinal spin Seebeck effect (LSSE) and $E_{\mathrm{ANE}} = S_{\mathrm{ANE}} \nabla_T \times M$ induced by anomalous Nernst effect (ANE) can offer thermoelectric contributions during the HHVR measurement, where the D_{ISHE} and S_{ANE} are the inverse spin-Hall effect and ANE coefficients, respectively [30–33]. In our system, the thermoelectric signal caused by ∇_T^z was inseparable because of the same manifestation ($J_s \parallel \nabla_T$ and $\sigma \parallel M$), while the ∇_T^x generated thermoelectric contribution comes only from the ANE of Co layer and LSSE is forbidden for $J_s \parallel \sigma$. As a result, the ∇_T^z is unavoidable because of large difference of thermal conductivity between SiO_2 ($\kappa = 1.4$ W m^{-1} K^{-1}) and air ($\kappa = 0.024$ W m^{-1} K^{-1}) [see Fig. 3(a)], whereas ∇_T^x mainly comes from the asymmetry of the structure and does not affect the estimation of SOT effective fields [see Fig. 3(b) and Sec. S8 in the Supplemental Material] [22].

For simplicity, we define the thermoelectric resistance $R_{\nabla_T}^z$ as R_{ANE} since the LSSE is smaller than the ANE in metallic HM/FM bilayers [27,34]. Figure 3(c) shows the linear dependence of $|R_{\mathrm{ANE}}|$ on current (I) for different Pt thick samples, which confirms the resistance is indeed caused by the thermoelectric effect, since $V_{\mathrm{ANE}} \propto \nabla T \propto I^2 R$ hence $R_{\mathrm{ANE}} \propto I$. Compared with the pure Pt sample, the multilayer samples

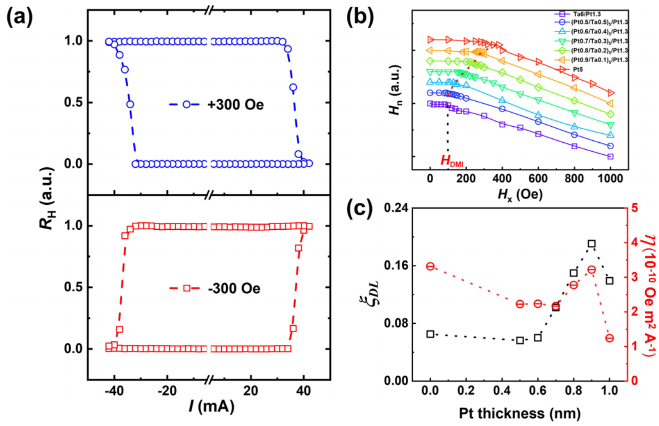

FIG. 4. (a) Current-induced SOT switching under in-plane magnetic field $H_x = \pm 300$ Oe for sample with $t_{Pt} = 0.9$. (b) Nucleation field H_n (extracted from the polar MOKE) as a function of in-plane field H_x for different Pt thickness films. The DMI field (H_{DMI}) is defined as corresponding H_x when the H_n begins to descend. (c) ξ_{DL} and η dependence of samples with different t_{Pt}.

with different t_{Pt} show the larger thermoelectric signals due to the higher thermal power and larger temperature gradient $\nabla_z^{Co}T$ in the Co layer caused by increased resistivity of HM layers and shunt effect, respectively. We used the finite element analysis method to accurately analyze the $\nabla_z^{Co}T$ of Pt/Ta multilayer samples. The detailed material parameters and simulation conditions are summarized in Sec. S9 in the Supplemental Material [22]. As shown in Fig. 3(d), the $\nabla_z^{Co}T$ increases continuously with increasing resistance of HM layer. It worth noting that the HM layer resistance of pure Pt sample in Fig. 3(d) is higher than that of multilayer samples with $t_{Pt} = 0.8$ and 0.9, which is due to the thicker HM layer for the latter and the limitation of the parallel resistance model. In our work, the resistivities of the multilayer samples are all much higher than that of pure Pt sample and thus have higher $\nabla_z^{Co}T$ as expected. The R_{ANE} of Ta (6)/Pt (1.3) bilayer is lower compared to that of other t_{Pt} samples despite its higher resistance, which may be related to its smaller S_{ANE}. We also performed the current versus longitudinal resistance R_{xx} and the temperature versus R_{xx} measurements to carefully calibrate the device temperature rise when current passed through the Pt/Ta multilayer samples, see Sec. S10 in the Supplemental Material [22]. Compared with the pure Pt sample (~307 K at 10 mA), the multilayer samples showed a higher temperature rise for the same applied current (~316 K at 10 mA), which is consistent with the results of finite element analysis.

For micron-sized Hall bar devices, SOT-induced magnetization switching and domain wall motion are widely considered as SHE + DMI scenarios [35,36]. We performed deterministic SOT magnetization switching under H_x, here the H_x is set to equal to or slightly larger than the DMI field. Figure 4(a) shows the deterministic magnetization switching of sample with $t_{Pt} = 0.9$. The DMI field (H_{DMI}) of samples with different t_{Pt} can be determined by the method based on the magnetic droplet nucleation model [37]. Using a polar magneto-optical Kerr effect (MOKE) microscopy, H_{DMI} is defined as the corresponding H_x value at the beginning of nucleation field (H_n) descent.

In Fig. 4(b), the H_{DMI} can be continuously tuned from ≈ 400 Oe (pure Pt sample) to ≈ 100 Oe (Ta (6)/Pt (1.3) sample) with decreasing t_{Pt}, which is similar to previous work on Pt/(CoFeB/CoFe)/MgO and Ta/(CoFeB/CoFe)/MgO heterojunctions [35,38]. We then calculated DMI exchange constant $|D|$ for Pt/Ta multilayers via $|D| = \mu_o M_S \Delta \, |H_{DMI}|$, where Δ is domain wall width and relates to exchange stiffness constant A with $\Delta = \sqrt{A/K_{u,\mathrm{eff}}}$, where $K_{u,\mathrm{eff}}$ is the effective perpendicular magnetic anisotropy energy density. Taking $A \approx 1.5 \times 10^{-11}$J/m [39], we obtained the t_{Pt} dependence of estimated $|D|$ (see Sec. S11 in the Supplemental Material) [22]. With reducing t_{Pt}, $|D|$ decreases gradually from ≈ 0.35 mJ/m^2 to ≈ 0.06 mJ/m^2, which is agreement with the variation of H_{DMI}. Tacchi *et al.* reported the interfacial DMI enhances with the increase of t_{Pt}, and finally saturates at approximately 0.45 mJ/m^2 when t_{Pt} is around 2 nm [40]. Similar results were also demonstrated for DMI in Ta/Pt bilayers by Kim *et al.* and Chen *et al.* [41,42]. Since D signs of Ta and Pt are opposite, with the Pt thickness increases, D first gradually decreases and undergoes a sign transition, and finally reaches saturation when t_{Pt} is approximately 2.4 and 3 nm, respectively [41,42]. In our Pt/Ta multilayers, the thickness of Pt in contact with Co is 1.3 nm. Thus, the interfacial DMI exchange constant could be also affected by the underlying Pt/Ta submonolayers. The decrease of t_{Pt} (increase of t_{Ta}) leads to gradual weakening of D and hence the H_{DMI}.

We then calculated the SOT switching efficiency $\eta = H_p/J_c$ as shown in Fig. 4(c) where the H_p is the depinning field and J_c is the critical switching current density [26,43,44]. The switching mechanism of devices can be elucidated via domain wall nucleation and propagation (see Sec. S12 in the Supplemental Material) [22,45,46] and the ξ_{DL} and η have similar variation trends with the change of t_{Pt}.

In summary, we have systematically investigated SOT efficiency of Pt/Ta multilayers using harmonic methods. We clarified that the contradictory results for low-field and high-field methods is attributed to the thermoelectric effect generated by the ∇_T^z in Pt/Ta multilayers. Combined with finite element simulation, we demonstrated that the enhanced thermoelectric effect is due to the shunt effect caused by the increase of HM resistivities and the change of S_{ANE} of multilayer structures. Moreover, the ξ_{DL} and DMI field can be continuously tunable by changing t_{Pt}. Our work provides a HM system with tunable SOT strength and confirms the significant thermoelectric effect in HM multilayer/FM structures, which will offer accurate measurement of SOT strength.

ACKNOWLEDGMENTS

This work was supported by the National Key R&D Program of China (Grant No. 2022YFA1405102), the National Natural Science foundation of China (Grant No. 12241405), the Chinese Academy of Sciences (Grants No. XDB28000000 and No. XDB44000000), the Beijing Natural Science Foundation (Grant No. 2212048), and the Beijing Natural Science Foundation Key Program (Grant No. Z190007).

[1] I. M. Miron, K. Garello, G. Gaudin, P.-J. Zermatten, M. V. Costache, S. Auffret, S. Bandiera, B. Rodmacq, A. Schuhl, and P. Gambardella, Perpendicular switching of a single ferromagnetic layer induced by in-plane current injection, Nature (London) **476**, 189 (2011).

[2] L. Liu, C.-F. Pai, Y. Li, H. W. Tseng, D. C. Ralph, and R. A. Buhrman, Spin-torque switching with the giant spin hall effect of tantalum, Science **336**, 555 (2012).

[3] K. Cai, M. Yang, H. Ju, S. Wang, Y. Ji, B. Li, K. W. Edmonds, Y. Sheng, B. Zhang, N. Zhang, S. Liu, H. Zheng, and K. Wang, Electric field control of deterministic current-induced magnetization switching in a hybrid ferromagnetic/ferroelectric structure, Nat. Mater. **16**, 712 (2017).

[4] Y. Cao, Y. Sheng, K. W. Edmonds, Y. Ji, H. Zheng, and K. Wang, Deterministic magnetization switching using lateral spin–orbit torque, Adv. Mater. **32**, 1907929 (2020).

[5] X. H. Liu, K. W. Edmonds, Z. P. Zhou, and K. Y. Wang, Tuning Interfacial Spins in Antiferromagnetic–Ferromagnetic–Heavy-Metal Heterostructures Via Spin-Orbit Torque, Phys. Rev. Appl. **13**, 014059 (2020).

[6] L. Liu, O. J. Lee, T. J. Gudmundsen, D. C. Ralph, and R. A. Buhrman, Current-Induced Switching of Perpendicularly Magnetized Magnetic Layers Using Spin Torque from the Spin Hall Effect, Phys. Rev. Lett. **109**, 096602 (2012).

[7] M. Yang, K. Cai, H. Ju, K. W. Edmonds, G. Yang, S. Liu, B. Li, B. Zhang, Y. Sheng, S. Wang, Y. Ji, and K. Wang, Spin-orbit torque in Pt/CoNiCo/Pt symmetric devices, Sci. Rep. **6**, 20778 (2016).

[8] X. Qiu, K. Narayanapillai, Y. Wu, P. Deorani, D.-H. Yang, W.-S. Noh, J.-H. Park, K.-J. Lee, H.-W. Lee, and H. Yang, Spin–orbit-torque engineering via oxygen manipulation, Nat. Nanotechnol. **10**, 333 (2015).

[9] A. R. Mellnik, J. S. Lee, A. Richardella, J. L. Grab, P. J. Mintun, M. H. Fischer, A. Vaezi, A. Manchon, E.-A. Kim, N. Samarth, and D. C. Ralph, Spin-transfer torque generated by a topological insulator, Nature (London) **511**, 449 (2014).

[10] S. C. Baek, V. P. Amin, Y.-W. Oh, G. Go, S.-J. Lee, G.-H. Lee, K.-J. Kim, M. D. Stiles, B.-G. Park, and K.-J. Lee, Spin currents and spin-orbit torques in ferromagnetic trilayers, Nat. Mater. **17**, 509 (2018).

[11] E. Zhang, Y. Deng, W. Li, X. Liu, and K. Wang, Enhancing spin-orbit torque efficiency via optimizing Pt-based multilayers, Phys. Status Solidi **219**, 2200498 (2022).

[12] Z. A. Bekele, X. Liu, Y. Cao, and K. Wang, High-efficiency spin-orbit torque switching using a single heavy-metal alloy with opposite spin hall angles, Adv. Electron. Mater. **7**, 2000793 (2021).

[13] Z. A. Bekele, R. Li, Y. Li, Y. Cao, X. Liu, and K. Wang, Tuning the high-efficiency field-free current-induced deterministic switching via ultrathin PtMo layer with Mo content, Adv. Electron. Mater. **7**, 2100528 (2021).

[14] X. Qiu, P. Deorani, K. Narayanapillai, K.-S. Lee, K.-J. Lee, H.-W. Lee, and H. Yang, Angular and temperature dependence of current induced spin-orbit effective fields in Ta/CoFeB/MgO nanowires, Sci. Rep. **4**, 4491 (2015).

[15] L. Liu, T. Moriyama, D. C. Ralph, and R. A. Buhrman, Spin-Torque Ferromagnetic Resonance Induced by the Spin Hall Effect, Phys. Rev. Lett. **106**, 036601 (2011).

[16] M.-H. Nguyen, D. C. Ralph, and R. A. Buhrman, Spin Torque Study of the Spin Hall Conductivity and Spin Diffusion Length in Platinum Thin Films with Varying Resistivity, Phys. Rev. Lett. **116**, 126601 (2016).

[17] P. He, X. Qiu, V. L. Zhang, Y. Wu, M. H. Kuok, and H. Yang, Continuous tuning of the magnitude and direction of spin-orbit torque using bilayer heavy metals, Adv. Electron. Mater. **2**, 1600210 (2016).

[18] Q. Ma, Y. Li, D. B. Gopman, Y. P. Kabanov, R. D. Shull, and C. L. Chien, Switching a Perpendicular Ferromagnetic Layer by Competing Spin Currents, Phys. Rev. Lett. **120**, 117703 (2018).

[19] Y. Liu, X. Liu, and J.-G. Zhu, Tailoring the current-driven domain wall motion by varying the relative thickness of two heavy metal underlayers, IEEE Trans. Magn. **54**, 4300305 (2018).

[20] E. Z. Zhang, Y. C. Deng, X. H. Liu, X. Z. Zhan, T. Zhu, and K. Y. Wang, Manipulating antiferromagnetic interfacial states by spin-orbit torques, Phys. Rev. B **104**, 134408 (2021).

[21] M. Hayashi, J. Kim, M. Yamanouchi, and H. Ohno, Quantitative characterization of the spin-orbit torque using harmonic all voltage measurements, Phys. Rev. B **89**, 144425 (2014).

[22] See Supplemental Material at http://link.aps.org/supplemental/10.1103/PhysRevB.107.214440 for low-field harmonic technique for PMA system (Fig. S1); low-field and high-field harmonic results of Pt/Co/Ru and W/CoFeB/MgO samples (Fig. S2); effective magnetic anisotropy field and coercivity of Pt/Ta multilayer systems (Fig. S3); PHE correction of Pt/Ta multilayer systems (Figs. S4 and S5); angle dependence of low-field and high-field harmonic results in Pt/Ta multilayers (Figs. S6 and S7); high-field harmonic results of Pt/Ta multilayer systems (Fig. S8); the resistivity of Pt/Ta multilayer systems (Fig. S9); anomalous Nernst resistance induced by thermal gradient in x direction (Fig. S10); finite element analysis of Pt/Ta multilayer systems (Fig. S11); the evaluation of the Joule heating in Pt/Ta multilayers (Fig. S12); DMI exchange constants of Pt/Ta multilayers (Fig. S13); magnetization switching via domain wall nucleation and propagation (Fig. S14), which includes Refs. [21,23,24,27,45,46].

[23] C.-F. Pai, L. Liu, Y. Li, H. W. Tseng, D. C. Ralph, and R. A. Buhrman, Spin transfer torque devices utilizing the giant spin hall effect of tungsten, Appl. Phys. Lett. **101**, 122404 (2012).

[24] L. Zhu, K. Sobotkiewich, X. Ma, X. Li, D. C. Ralph, and R. A. Buhrman, strong dampinglike spin-orbit torque and tunable dzyaloshinskii–moriya interaction generated by low-resistivity $Pd_{1-x}Pt_x$ alloys, Adv. Funct. Mater. **29**, 1805822 (2019).

[25] P. M. Haney, H.-W. Lee, K.-J. Lee, A. Manchon, and M. D. Stiles, Current induced torques and interfacial spin-orbit coupling: semiclassical modeling, Phys. Rev. B **87**, 174411 (2013).

[26] T.-Y. Chen, C.-T. Wu, H.-W. Yen, and C.-F. Pai, Tunable spin-orbit torque in Cu-Ta binary alloy heterostructures, Phys. Rev. B **96**, 104434 (2017).

[27] C. O. Avci, K. Garello, M. Gabureac, A. Ghosh, A. Fuhrer, S. F. Alvarado, and P. Gambardella, Interplay of spin-orbit torque and thermoelectric effects in ferromagnet/normal-metal bilayers, Phys. Rev. B **90**, 224427 (2014).

[28] L. Zhu, J. Li, L. Zhu, and X. Xie, Boosting Spin-Orbit-Torque Efficiency in Spin-Current-Generator/Magnet/Oxide Superlattices, Phys. Rev. Appl. **18**, 064052 (2022).

[29] T. Shirokura and P. N. Hai, Angle resolved second harmonic technique for precise evaluation of spin orbit torque in strong perpendicular magnetic anisotropy systems, Appl. Phys. Lett. **119**, 222402 (2021).

[30] L. Berger, Application of the side-jump model to the hall effect and nernst effect in ferromagnets, Phys. Rev. B **5**, 1862 (1972).

[31] J. Weischenberg, F. Freimuth, S. Blügel, and Y. Mokrousov, Scattering-independent anomalous Nernst effect in ferromagnets, Phys. Rev. B **87**, 060406(R) (2013).

[32] A. Azevedo, L. H. Vilela Leão, R. L. Rodriguez-Suarez, A. B. Oliveira, and S. M. Rezende, Dc effect in ferromagnetic resonance: Evidence of the spin-pumping effect? J. Appl. Phys. **97**, 10C715 (2005).

[33] E. Saitoh, M. Ueda, H. Miyajima, and G. Tatara, Conversion of spin current into charge current at room temperature: Inverse spin-Hall effect, Appl. Phys. Lett. **88**, 182509 (2006).

[34] S. Y. Huang, W. G. Wang, S. F. Lee, J. Kwo, and C. L. Chien, Intrinsic Spin-Dependent Thermal Transport, Phys. Rev. Lett. **107**, 216604 (2011).

[35] C.-F. Pai, M. Mann, A. J. Tan, and G. S. D. Beach, Determination of spin torque efficiencies in heterostructures with perpendicular magnetic anisotropy, Phys. Rev. B **93**, 144409 (2016).

[36] S. Emori, U. Bauer, S.-M. Ahn, E. Martinez, and G. S. D. Beach, Current-driven dynamics of chiral ferromagnetic domain walls, Nat. Mater. **12**, 611 (2013).

[37] S. Kim, P.-H. Jang, D.-H. Kim, M. Ishibashi, T. Taniguchi, T. Moriyama, K.-J. Kim, K.-J. Lee, and T. Ono, Magnetic droplet nucleation with a homochiral néel domain wall, Phys. Rev. B **95**, 220402(R) (2017).

[38] S. Emori, E. Martinez, K.-J. Lee, H.-W. Lee, U. Bauer, S.-M. Ahn, P. Agrawal, D. C. Bono, and G. S. D. Beach, Spin hall torque magnetometry of Dzyaloshinskii domain walls, Phys. Rev. B **90**, 184427 (2014).

[39] P. J. Metaxas, J. P. Jamet, A. Mougin, M. Cormier, J. Ferré, V. Baltz, B. Rodmacq, B. Dieny, and R. L. Stamps, Creep and Flow Regimes of Magnetic Domain-Wall Motion in Ultrathin Pt/Co/Pt Films with Perpendicular Anisotropy, Phys. Rev. Lett. **99**, 217208 (2007).

[40] S. Tacchi, R. E. Troncoso, M. Ahlberg, G. Gubbiotti, M. Madami, J. Åkerman, and P. Landeros, Interfacial Dzyaloshinskii-Moriya Interaction in Pt/Cofeb Films: Effect of the Heavy-Metal Thickness, Phys. Rev. Lett. **118**, 147201 (2017).

[41] N.-H. Kim, D.-S. Han, J. Jung, K. Park, H. J. M. Swagten, J.-S. Kim, and C.-Y. You, Dependence of interfacial Dzyaloshinskii-Moriya interaction and perpendicular magnetic anisotropy on the thickness of the heavy-metal layer, Appl. Phys. Express **10**, 103003 (2017).

[42] Y. Chen, Q. Zhang, J. Jia, Y. Zheng, Y. Wang, X. Fan, and J. Cao, Tuning Slonczewski-like torque and Dzyaloshinskii-Moriya interaction by inserting a Pt spacer layer in Ta/CoFeB/MgO structures, Appl. Phys. Lett. **112**, 232402 (2018).

[43] R. Mishra, J. Yu, X. Qiu, M. Motapothula, T. Venkatesan, and H. Yang, Anomalous Current-Induced Spin Torques in Ferrimagnets near Compensation, Phys. Rev. Lett. **118**, 167201 (2017).

[44] O. J. Lee, L. Q. Liu, C. F. Pai, Y. Li, H. W. Tseng, P. G. Gowtham, J. P. Park, D. C. Ralph, and R. A. Buhrman, Central role of domain wall depinning for perpendicular magnetization switching driven by spin torque from the spin hall effect, Phys. Rev. B **89**, 024418 (2014).

[45] K. R. Coffey, T. Thomson, and J.-U. Thiele, Angular dependence of the switching field of thin-film longitudinal and perpendicular magnetic recording media, J. Appl. Phys. **92**, 4553 (2002).

[46] F. Schumacher, On the modification of the Kondorsky function, J. Appl. Phys. **70**, 3184 (1991).